EDGE ARTICLE

Check for updates

The simplest structure of a stable radical showing high fluorescence efficiency in solution: benzene donors with triarylmethyl radicals†

Yohei Hattori, [ID] *[a] Ryota Kitajima,[a] Wataru Ota,[b] Ryota Matsuoka, [ID] [cd] Tetsuro Kusamoto, [ID] [cde] Tohru Sato[fg] and Kingo Uchida [ID] [a]

Donor–radical acceptor systems have recently attracted much attention as efficient doublet emitters that offer significant advantages for applications such as OLEDs. We employed an alkylbenzene (mesityl group) as the simplest donor to date and added it to a diphenylpyridylmethyl radical acceptor. The (3,5-difluoro-4-pyridyl)bis[2,6-dichloro-4-(2,4,6-trimethylphenyl)phenyl]methyl radical (Mes_2F_2PyBTM) was prepared in only three steps from commercially available reagents. A stable radical composed of only one pyridine ring, four benzene rings, methyl groups, halogens, and hydrogens showed fluorescence of over 60% photoluminescence quantum yield (PLQY) in chloroform, dichloromethane, and PMMA. The key to high fluorescence efficiency was benzene rings perpendicular to the diphenylpyridylmethyl radical in the doublet ground (D_0) state. The relatively low energy of the β-HOMO and the electron-accepting character of the radical enabled the use of benzenes as electron donors. Furthermore, the structural relaxation of the doublet lowest excited (D_1) state was minimized by steric hindrance of the methyl groups. The reasons for this high efficiency include the relatively fast fluorescence transition and the slow internal conversion, both of which were explained by the overlap density between the D_1 and D_0 states.

Introduction

Recently, stable radicals have attracted much interest as luminescent materials.[1,2] The key to their luminescence is the fluorescence from the D_1 state to the D_0 state. In contrast to the singlet lowest excited (S_1) state of closed-shell molecules, which is higher in energy than the triplet lowest excited state (T_1), it is normal for the energy of the D_1 state to be lower than that of the quartet lowest excited (Q_1) state. Therefore, the fluorescence of radicals can avoid unfavorable quenching from higher multiplicity excited states produced by the recombination of electrons and holes or intersystem crossing from the S_1 state. Stable luminescent radicals are one of the most promising substance

groups of emitters suitable for highly efficient electroluminescent (EL) devices.[3,4] A relatively basic application would be use in a heavy atom environment.[5,6]

Problems due to thermal stability of the radicals had been resolved with the invention of polychlorotriphenylmethyl radicals such as perchlorotriphenylmethyl radical (PTM)[7] and tris(2,4,6-trichlorophenyl)methyl radical (TTM).[8] For a luminescent material, higher stability, that is, stability under photoexcitation conditions (photostability), is necessary; however, the photodecomposition of PTM and TTM had been reported.[9,10] We have reported that the introduction of a pyridyl group instead of a phenyl group has greatly improved the stability of the radical under photoirradiation.[11] Compared with TTM, the (3,5-dichloro-4-pyridyl)bis(2,4,6-trichlorophenyl) methyl radical (PyBTM) showed *ca.* 70 times higher photostability in dichloromethane.

Dilute PyBTM doped in (3,5-dichloro-4-pyridyl)bis(2,4,6-trichlorophenyl)methane (αH-PyBTM) crystal had an excellent feature of high fluorescence efficiency (Φ_f = 89%).[12] In molecular solids of stable radicals, spin-derived properties such as magnetism are important properties,[13] and PyBTM has been used to investigate interesting photophysical phenomena such as the coherent coupling between spin ensembles,[14] a magnetic field effect on luminescence (magnetoluminescence),[12,15,16] and photoluminescence anisotropy amplified by exciton funneling.[17] However, the fluorescence efficiency of PyBTM was low in liquid solutions, similar to other simple triarylmethyl

[a]Materials Chemistry Course, Faculty of Advanced Science and Technology, Ryukoku University, Seta, Otsu, Shiga 520-2194, Japan. E-mail: hattori@rins.ryukoku.ac.jp

[b]MOLFEX, Inc., Takano-Nishibiraki-cho 34-4, Kyoto 606-8103, Japan

[c]Department of Life and Coordination-Complex Molecular Science, Institute for Molecular Science, 5-1, Higashiyama, Myodaiji, Okazaki, Aichi 444-8787, Japan

[d]SOKENDAI (The Graduate University for Advanced Studies), Shonan Village, Hayama, Kanagawa 240-0193, Japan

[e]JST-PRESTO, 4-1-8, Honcho, Kawaguchi, Saitama 332-0012, Japan

[f]Fukui Institute for Fundamental Chemistry, Kyoto University, Takano-Nishibiraki-cho 34-4, Kyoto 606-8103, Japan

[g]Department of Molecular Engineering, Graduate School of Engineering, Kyoto University, Nishikyo-ku, Kyoto 615-8510, Japan

† Electronic supplementary information (ESI) available. See DOI: https://doi.org/10.1039/d2sc05079j

radicals. The PLQYs of PyBTM and TTM were both 2% in dichloromethane and 3% in chloroform.[11] Introduction of fluorine atoms on the pyridine ring slightly improved the PLQY in solution, and the (2,5-difluoro-4-pyridyl)bis(2,4,6-trichlorophenyl)methyl radical (F$_2$PyBTM) showed PLQY of 4% in dichloromethane and 6% in chloroform.[18] Utilizing the coordination ability of a nitrogen atom on the pyridine ring, we have developed Au^I complexes of PyBTM derivatives and improved the fluorescence efficiency to 36%.[19–21]

On the other hand, the PLQYs of PTM or TTM derivatives have been improved by constructing a donor–acceptor system using nitrogen-containing electron donors such as carbazoles[22–26] or triphenylamines.[25,27] Highly fluorescent radicals showing PLQY above 50% in solution were first reported as a carbazole donor–TTM radical acceptor system showing 53% PLQY in cyclohexane.[22] However, its fluorescence was quenched by the polarity of solvent molecules to 2% in chloroform. By adding electron-withdrawing groups on carbazole, strong fluorescence was maintained in chloroform.[24] It is noteworthy that efficient fluorescence in more polar solvents has recently been reported in completely different systems: pyrene-dithiadiazolyl radical (Φ_f = 50% in acetonitrile)[28] and the π-radical stabilized with boron (Φ_f = 67% in DMF).[29]

Here, we report that simple aromatic hydrocarbons, mesityl groups, work as donors, and significantly enhance the fluorescence efficiencies of PyBTM and F$_2$PyBTM in dichloromethane and chloroform solutions. We explain the reasons for the high efficiencies of these nonplanar π-electron systems by photophysical theories and calculations using DFT and TD-DFT.

Results and discussion

From commercially available reagents, αH-PyBTM[11] and (3,5-difluoro-4-pyridyl)bis(2,4,6-trichlorophenyl)methane (αH-F$_2$PyBTM)[18] were prepared in one step (Scheme 1). In the second step, the Suzuki–Miyaura coupling reaction with a micellar

catalysis[30] and 2,4,6-trimethylphenylboronic acid selectively yielded mesityl substituents at the *para* position. The stable radicals MesPyBTM, Mes$_2$PyBTM, and Mes$_2$F$_2$PyBTM were synthesized by deprotonation and oxidation processes. Thus, these radicals were all prepared in three steps from commercially available reagents. ESR spectra revealed that these radicals have S = 1/2 spin on one molecule (Fig. S1†).

These radicals were stable under ambient conditions similar to other triarylmethyl radicals protected by halogen atoms.[7,8] Actually, these radicals were purified by chromatography on silica gel under ambient conditions, and their melting points could be determined. All the spectroscopic measurements were conducted under ambient conditions as no effect due to oxygen was observed similar to the other PyBTM derivatives,[5,11,18–21] probably due to short fluorescence lifetimes. As with PyBTM,[11] no change was observed in the solutions stored in the dark.

Absorption and emission spectra of MesPyBTM and Mes$_2$-PyBTM in dichloromethane are compared with those of PyBTM and (3,5-dichloro-4-pyridyl)bis(2,6-dichloro-4-phenylphenyl) methyl radical (PyPBTM)[30] in Fig. 1a. The absorption spectrum of PyPBTM was clearly different from that of PyBTM, and both the α-HOMO–α-LUMO band (λ_{max} = 370 → 401 nm) and the β-HOMO–β-LUMO band (541 → 564 nm) were significantly redshifted. On the other hand, the shapes of the absorption spectra of MesPyBTM and Mes$_2$PyBTM were rather similar to that of PyBTM with the same absorption maxima at λ_{max} = 370 and 541 ($\pm$1) nm. This result is attributed to the only slightly changed energy levels of the frontier orbitals.

This occurs because the mesityl group has bulky methyl groups at *ortho* positions and can barely conjugate with π-orbitals on the neighboring phenyl group. In order to estimate structures using DFT, we adopted the UB3LYP level of theory with 6-31G(d, p) basis sets, since they closely reproduced the experimental absorption and emission spectra from previous studies.[11,19–21,31] The solvent effect of dichloromethane was taken into account by using a polarizable continuum model (PCM).[32,33] The dihedral angle between the mesityl and dichlorophenyl groups was 83° for MesPyBTM and 84° for Mes$_2$PyBTM in the DFT optimized D$_0$ state model (Table S1†). These are nearly perpendicular in contrast to the rather flat angles (34°) between the phenyl and dichlorophenyl groups in PyPBTM.

Redshifts of emission from PyBTM (λ_{em} = 585 nm) were seen in MesPyBTM (λ_{em} = 645 nm) and Mes$_2$PyBTM (λ_{em} = 628 nm), although these shifts were smaller than that of PyPBTM (λ_{em} = 654 nm). In the TD-DFT (UB3LYP/6-31G(d, p)) optimized D$_1$ structure, the mesityl groups under the β-HOMO are electron-deficient, and the dihedral angle decreased to 50° to conjugate to the relatively electron-rich dichlorophenyl group (Table S1†). This structural relaxation was the cause of this redshift. The dihedral angle became even smaller in PyPBTM, decreasing to 25°.

Absorption and emission spectra of Mes$_2$F$_2$PyBTM and F$_2$PyBTM are shown in Fig. 1b. The shape of the absorption spectrum of Mes$_2$F$_2$PyBTM (λ_{max} = 352 nm) resembles that of F$_2$PyBTM (λ_{max} = 351 nm). The dihedral angle between the mesityl and dichlorophenyl groups was 87° in the DFT

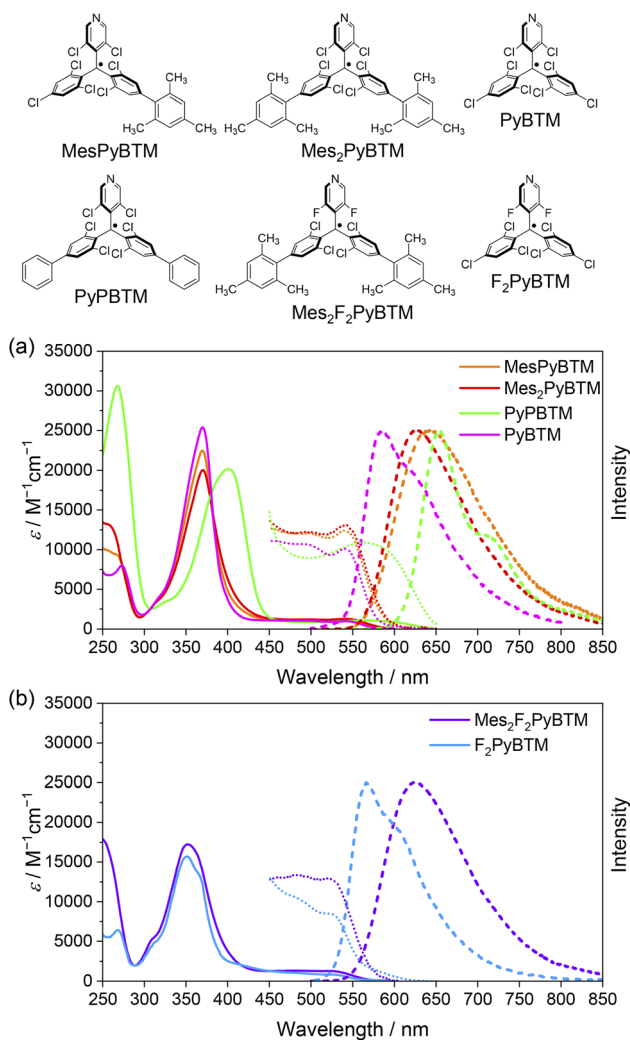**Scheme 1** Synthesis of MesPyBTM, Mes$_2$PyBTM, and Mes$_2$F$_2$PyBTM.
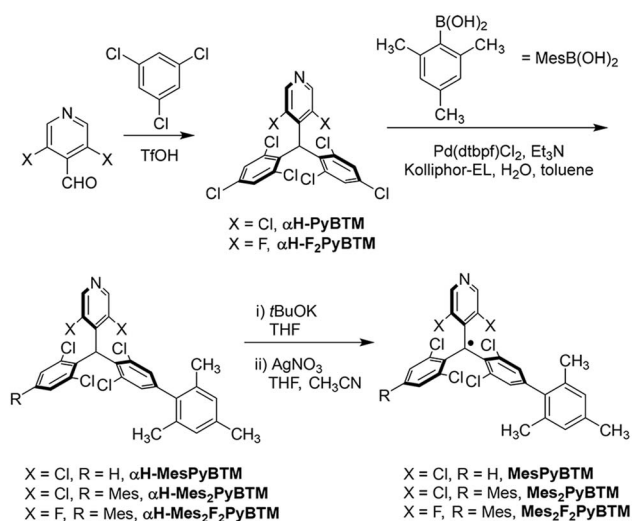
Fig. 1 (a) Absorption (solid line) and emission (broken line, $\lambda_{ex} = 450$ nm) spectra of MesPyBTM (orange), Mes$_2$PyBTM (red), PyPBTM (light green), and PyBTM (pink) in dichloromethane. Enlarged portions of the absorption spectra (10 fold) are shown from $\lambda = 450$ to 650 nm (dotted lines). The concentration of MesPyBTM, Mes$_2$PyBTM, PyPBTM, and PyBTM was 7.2×10^{-5}, 7.7×10^{-5}, 2.0×10^{-5}, and 2.5×10^{-5} M, respectively. (b) Absorption (solid line) and emission (broken line, $\lambda_{ex} = 450$ nm) spectra of Mes$_2$F$_2$PyBTM (purple) and F$_2$PyBTM (light blue) in dichloromethane. Enlarged portions of the absorption spectra (10 fold) are shown from $\lambda = 450$ to 650 nm (dotted lines). The concentration of Mes$_2$F$_2$PyBTM and F$_2$PyBTM was 6.2×10^{-5} and 2.5×10^{-5} M, respectively.

Table 1 PLQYs and photophysical parameters of radicals in dichloromethane

	λ_{em} (nm)	Φ_f (%)	τ/ns	$k_f/10^7$ s^{-1}	$k_{nr}/10^7$ s^{-1}
PyBTM[a]	585	2	6.4	0.3	14
F$_2$PyBTM[b]	566	4	12.5	0.3	7.7
PyPBTM	654	9.5	12	0.8	7.5
MesPyBTM	645	30	26	1.2	2.7
Mes$_2$PyBTM	628	47	38	1.2	1.4
Mes$_2$F$_2$PyBTM	623	66	44	1.5	0.8

[a] Cited from ref. 11. [b] Cited from ref. 18. All Φ_fs were obtained by absolute PLQY measurement.

efficiency of the radical, and the effect was much larger than that by the phenyl groups. The PLQY of 2% for PyBTM was elevated to 30% by the addition of a mesityl group and to 47% by double substitution of mesityl groups. In particular, Mes$_2$-F$_2$PyBTM displayed as much as 66% PLQY in dichloromethane, and 69% in chloroform (Fig. S2†). As far as we know, a higher PLQY of the fluorescent radical in a liquid solution has only been reported for pyridoindole donor–TTM acceptor systems in 2020[34] and 2022[35] and the π-radical stabilized with boron in 2022.[29]

The major structural difference between pyridoindole donor–TTM acceptor systems[34,35] and Mes$_2$F$_2$PyBTM is that the former has two nitrogen atoms in the donor and the latter has one nitrogen atom in the radical. In contrast, the TTM radical is made of a carbon skeleton and the mesityl group is a hydrocarbon. In terms of organic chemistry of nitrogen-containing aromatics, an indole ring is electron-rich and a pyridine ring is electron-deficient. A pyridoindole is thought to cancel out the two effects internally. The use of mesityl groups simplifies the situation and provides important scientific or economic insights.

The nitrogen atom in the radical was introduced to improve the photostability of the radical as described in the Introduction. The photostabilities of the new radicals were measured in dichloromethane under UV light (370 nm) irradiation. The decay of fluorescence is plotted in Fig. S3,† and the stabilities of the new radicals were of about the same order as that in PyBTM (Table S3†). The photostability of Mes$_2$F$_2$PyBTM was slightly higher than that of PyBTM. The photostability of PyBTM was ca. 70 times that of TTM and similar to that of TIPS pentacene.[36] Therefore, it was found that a reasonable degree of photostability of PyBTM could be maintained.

The availability of the radicals as fluorophores in polar solvents means that they are also useful in polymers having polar substituents. Poly(methyl methacrylate) (PMMA) is one of the most useful polymers in optical applications, and it has polar carboxyl groups that can quench the fluorescence of some donor–acceptor type fluorophores. Mes$_2$F$_2$PyBTM in a PMMA film displayed PLQY of 62%, proving its usefulness in this polymer.

As mentioned in the Introduction, the Q$_1$ state is higher in energy, and all of the excited states are thought to converge to

optimized D$_0$ state (Table S1†). The redshift of emission from F$_2$PyBTM ($\lambda_{em} = 566$ nm) was seen in Mes$_2$F$_2$PyBTM ($\lambda_{em} = 623$ nm), similar to the case of Mes$_2$PyBTM. The optimized dihedral angle between the mesityl group under the β-HOMO and the neighboring dichlorophenyl group was 49° in the DFT optimized D$_1$ state.

Bright reddish-orange fluorescence was observed when the solutions of new radicals were irradiated with a UV lamp. The PLQYs in dichloromethane are shown in Table 1, and the PLQYs in chloroform are shown in Table S2.† As observed, the addition of mesityl groups dramatically increased the fluorescence

the D_1 state in a short time. The PLQYs of the radicals are determined by competition between the rate of fluorescence (k_f) and the rate of nonradiative decay (k_{nr}) from the D_1 state (Fig. 2). Here, k_f and k_{nr} were calculated from the PLQYs and the fluorescence lifetimes (τ, Fig. S4†) of the radicals, and they are shown in Table 1.

One cause of the low PLQY of triarylmethyl radicals was the small k_f. The small transition dipole moment between D_1 and D_0 is interpreted as being caused by the C_3 symmetry of the molecule[37] or cancellation of the HOMO–SOMO and SOMO–LUMO transition dipole moments.[34] This barrier for emission is partially eliminated by constructing a donor–acceptor system. The β-HOMOs and β-LUMOs calculated using the TD-DFT (UB3LYP/6-31G(d, p)) at the optimized D_1 structure are shown in Fig. 2 (see also Fig. S5†). Since the D_1 states are mainly generated *via* the β-HOMO–β-LUMO transition, the radicals are regarded as a mesityl donor–PyBTM acceptor system. Experimentally, k_f in MesPyBTM, Mes$_2$PyBTM, and Mes$_2$F$_2$PyBTM was enhanced to a level 4 or 5 times that of PyBTM.

In 2020, Abdurahman *et al.* suggested that the large oscillator strength of a donor–acceptor system is due to intensity borrowing from the intense high-lying transition of the radical,[34] while Cho *et al.* showed that the k_f values are dominated by the coupling between the CT and ground state, and nearly independent of the donor strength.[38] We propose another view of the increase in k_f from visualization of the overlap density distribution by TD-DFT. Consideration of

interactions with local excitations is no longer necessary for intuitive understanding.

Within the crude adiabatic approximation,[39,40] we consider transitions from the initial vibronic state $|\Phi_{m\nu}\rangle = |\Psi_m\rangle|\chi_{m\nu}\rangle$ to the final one $|\Phi_{n\nu'}\rangle = |\Psi_n\rangle|\chi_{n\nu'}\rangle$, where $|\Psi_m\rangle$ ($|\Psi_n\rangle$) and $|\chi_{m\nu}\rangle$ ($|\chi_{n\nu'}\rangle$) are the initial (final) electronic and vibrational states, respectively. The initial and final vibronic energies are denoted as $E_{m\nu}$ and $E_{n\nu'}$, respectively. According to Fermi's golden rule, the rate constant of fluorescence from $|\Psi_m\rangle$ to $|\Psi_n\rangle$ is given by eqn (1).[41]

$$k_{n\leftarrow m}^{f} = \int_0^\infty d\omega \frac{4\omega^3}{3c^3}|\mu_{nm}|^2 \sum_{\nu,\nu'} P_{m\nu}(T)|\langle\chi_{n\nu'}|\chi_{m\nu}\rangle|^2 \delta$$
$$\left(E_{n\nu'} - E_{m\nu} + \hbar\omega\right) \quad (1)$$

where ω is the angular frequency of the photon, c is the speed of light, $P_{m\nu}(T)$ is the Boltzmann distribution function of $|\chi_{m\nu}\rangle$ at temperature T, μ_{nm} is the transition dipole moment between $|\Psi_m\rangle$ and $|\Psi_n\rangle$, and $\hbar$ is the Dirac constant. The radiative constant of fluorescence actually observed, $k_f = k_{0\leftarrow1}^{f}$ is proportional to the square of the transition dipole moment between the D_1 and D_0 states (μ_{10}).

A density form of the transition dipole moment ($\tau_{10}(\boldsymbol{x})$) is written as a product of a three-dimensional Cartesian coordinate ($\boldsymbol{x} = (x, y, z)$) and an overlap density between the D_1 and D_0 states ($\rho_{10}(\boldsymbol{x})$) as in eqn (2) and (3).[41,42]

$$\mu_{10} = \int d\boldsymbol{x}\, \tau_{10}(\boldsymbol{x}) \quad (2)$$

$$\tau_{10}(\boldsymbol{x}) = -e\boldsymbol{x}\rho_{10}(\boldsymbol{x}) \quad (3)$$

Thus, an overlap density having widespread distribution generally gives a large transition dipole moment. The calculated transition dipole moments of Mes$_2$PyBTM and Mes$_2$F$_2$PyBTM were larger than that of PyBTM (Table 2). This result was attributed to the overlap densities of Mes$_2$PyBTM and Mes$_2$F$_2$PyBTM delocalizing on both the PyBTM moiety and the mesityl group (Fig. 3).

The suppressed k_{nr} contributed to the high PLQY no less than the enhanced k_f. Since the only state lower in energy than the D_1 state is the ground state (D_0), the rate of intersystem crossing (k^{ISC}) to the other spin multiplet states is substantially zero, and 100% of k_{nr} is the rate constant of internal conversion (k^{IC}) to the D_0 state. Compared to the phenyl groups (PyPBTM), the relaxation of the D_1 state with the mesityl groups is sterically hindered by the methyl groups at the *ortho* positions. As
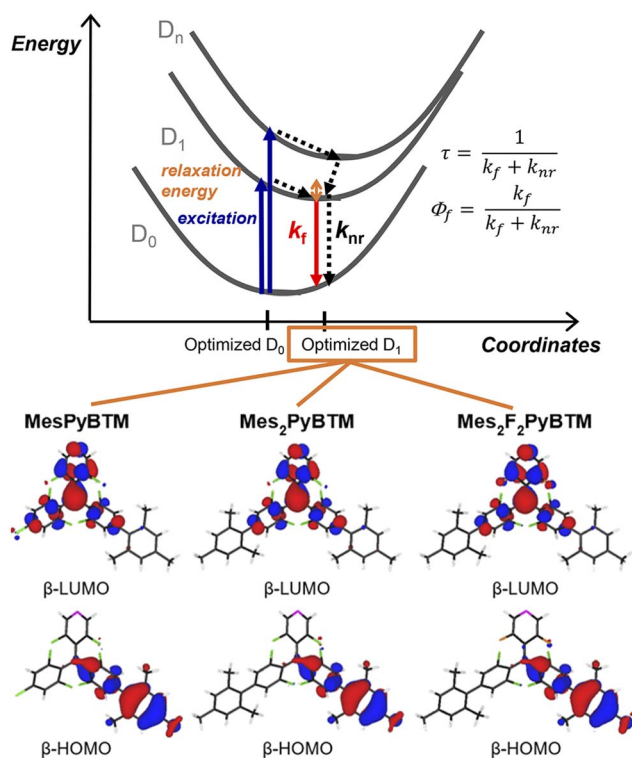

Fig. 2 Energy diagram for the D_1–D_0 fluorescence of the radicals and the β-HOMO and β-LUMO of MesPyBTM, Mes$_2$PyBTM, and Mes$_2$F$_2$-PyBTM at the D_1 optimized structure calculated using UB3LYP/6-31G(d, p).

Table 2 Calculated transition dipole moments between the D_1 and D_0 states in x, y, and z components of PyBTM, Mes$_2$PyBTM, and Mes$_2$F$_2$PyBTM at the D_1 optimized structure calculated using UB3LYP/6-31G(d, p)

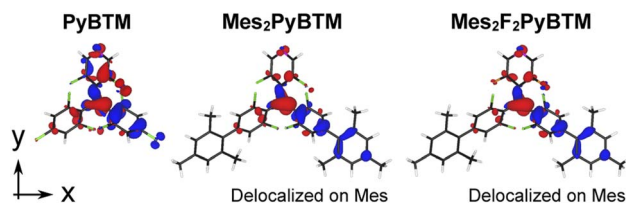|	$|\mu_{10}|$/a.u.		
	x	y	z
PyBTM	0.7012	0.3654	0.0725
Mes$_2$PyBTM	1.3525	0.7567	0.0451
Mes$_2$F$_2$PyBTM	1.2884	0.7722	0.0132

Fig. 3 Overlap densities between the D_1 and D_0 states of PyBTM, Mes$_2$PyBTM, and Mes$_2$F$_2$PyBTM. These were approximately given by the product of the β-HOMO and β-LUMO at the D_1 optimized structure.

a result, the energy of the D_1 state was raised and the internal conversion from D_1 to D_0 was slowed by the energy-gap law.[43] The fluorine atoms on the pyridine ring also have the effect of widening the D_1–D_0 gap,[18,20] and the record-small k_{nr} among diphenylpyridyl radicals was achieved in Mes$_2$F$_2$PyBTM.

In addition, the k^{IC} can also be discussed from the overlap density distribution. The rate constant of internal conversion from $|\Psi_m\rangle$ to $|\Psi_n\rangle$ is given by eqn (4).[41]

$$k_{n\leftarrow m}^{IC} = \frac{2\pi}{\hbar}\sum_{\alpha}|V_{nm,\alpha}|^2\sum_{\nu,\nu'}P_{m\nu}(T)|\langle\chi_{n\nu'}|Q_\alpha|\chi_{m\nu}\rangle|^2\delta\left(E_{n\nu'}-E_{m\nu}\right)$$

(4)

where $V_{nm,\alpha}$ is an off-diagonal vibronic coupling constant between $|\Psi_m\rangle$ and $|\Psi_n\rangle$ for the vibrational mode α, and Q_α is a mass-weighted normal coordinate. Here, k^{IC} is proportional to the square of the off-diagonal vibronic coupling constant (VCC) between the D_1 and D_0 states ($V_{10,\alpha}$ with α being a vibrational mode).

A density form of the off-diagonal VCC ($\eta_{10,\alpha}$) is written as a product of the overlap density and potential derivative ($\nu_\alpha(\boldsymbol{x})$) as in eqn (5) and (6).[41,42]

$$V_{10,\alpha} = \int d\boldsymbol{x}\ \eta_{10,\alpha}(\boldsymbol{x})$$

(5)

$$\eta_{10,\alpha}(\boldsymbol{x}) = \rho_{10}(\boldsymbol{x}) \times \nu_\alpha(\boldsymbol{x})$$

(6)

Note that the density forms of both the transition dipole moment and the off-diagonal VCC are expressed using the overlap density. Mes$_2$PyBTM and Mes$_2$F$_2$PyBTM have smaller off-diagonal VCCs than PyBTM (Fig. S6†) because their overlap densities are delocalized on the PyBTM moiety and on the mesityl group, which couple weakly to potential derivatives.

Conclusions

Enhancement of fluorescence by the addition of mesityl groups to PyBTM is explained from the viewpoint of the overlap density between the D_1 and D_0 states. In particular, Mes$_2$F$_2$PyBTM shows high fluorescence efficiency above 60% in dichloromethane, chloroform, and PMMA at room temperature under ambient conditions. Although the PLQY of 69% in chloroform is not the highest among those of luminescent radicals today,[29,34,35] this value is comparable to those of famous fluorescent dyes such as rhodamine B ($\Phi_f = 0.70$ in methanol,[44]

Fig. S7†). This paper has raised many important points: Simple benzene rings can behave as an electron-donor for electron-accepting PyBTM radicals, their fluorescence is not quenched in polar solvents due to their non-excessive electron-donating nature, and steric hindrance of the *ortho* methyl groups plays an important role in reducing internal conversion. Introducing a nitrogen atom into a radical without introducing a nitrogen atom into the donor is a reversal of the previous highly efficient stable luminescent radicals. This study will provide important clues about donor selection in donor–acceptor systems or non-planar fluorescent π-systems. We also expect that easily synthesized and highly fluorescent Mes$_2$PyBTM and Mes$_2$F$_2$PyBTM will be used in a variety of applications.

Experimental

Materials and methods

All reactions were carried out under an argon atmosphere. The starting materials, αH-PyBTM[11] and αH-F$_2$PyBTM,[18] were prepared according to the reference. Commercially available compounds were used as received without further purification. Preparative recycling gel permeation chromatography was performed with a recycling preparative HPLC, LaboACE LC-5060, Japan Analytical Industry Co., Ltd. ^{1}H (400 MHz) and ^{13}C NMR (100 MHz) spectra were recorded on a JEOL JNM-ECS 400 spectrometer using CDCl$_3$. The residual solvent signals (^{1}H NMR: δ 7.26, ^{13}C NMR: δ 77.16) were used as the internal standards. Elemental analysis was conducted at the Center for Organic Elemental Microanalysis, Graduate School of Pharmaceutical Sciences, Kyoto University. ESR spectra were recorded with a JEOL JES-FR30EX spectrometer with X-band microwave. Sample solutions were charged in a 2.5 mmϕ sample tube. Magnetic field was calibrated with the Mn^{2+}/MgO standard. Mass spectrometry was performed with a JEOL-JMS-S3000 (MALDI-Spiral-TOF MS) mass spectrometer with DCTB (20 mg mL^{-1} in CHCl$_3$) as a matrix and TFANa (1 mg mL^{-1} in THF) as a cationization agent. Melting points were measured on a Yanaco MP-500D. Absorption and emission spectra were monitored on a Hitachi U-4150 spectrophotometer and a Hitachi F-7100 fluorescence spectrophotometer, respectively. Photostability under 370 nm light was recorded with a JASCO FP-8600KS spectrofluorometer. Absolute luminescence quantum yields were measured using a Hamamatsu Photonics Quantaurus QY. Photoluminescence decay curves were measured using a measurement system with a picosecond diode laser with the emission wavelength of 375 nm (Advanced Laser Diode Systems PIL037X) as the light source, a single grating spectrometer (Andor Kymera193i-B1), and a photon counting detector (MPD SPD-050-CTE) operated using a time-correlated single photon counting (TCSPC) technique.

Preparation of emulsion

An emulsion of toluene in aqueous 2 wt% Kolliphor EL (K-EL) is prepared by mixing a 2 wt% aqueous dispersion of K-EL (1.8 g of K-EL in 88.2 mL of deionized water) with 10 mL of toluene until

a stable, milky dispersion is obtained. The emulsion and triethylamine were deoxygenated by bubbling argon before use.

Synthesis of αH-MesPyBTM and αH-Mes$_2$PyBTM

In a Schlenk tube, αH-PyBTM (783 mg, 1.50 mmol), 2,4,6-trimethylphenylboronic acid (746 mg, 4.55 mmol), and Pd(dtbpf)Cl$_2$ (79.3 mg, 0.122 mmol), were put under an argon atmosphere. The degassed K-EL 2 wt%: toluene (9 : 1 v/v) emulsion (3.5 mL) was added, and the mixture was heated at 70 °C. Degassed triethylamine (1.3 mL, 9.3 mmol) was finally added, and the reaction mixture was stirred at 70 °C overnight. The reaction mixture was cooled down to room temperature, dichloromethane was added, and filtered on a celite pad. The solvent was evaporated and purified by silica gel column chromatography (CHCl$_3$: hexane = 1 : 1). The crude product (742 mg) was separated by GPC (CHCl$_3$) to obtain pure αH-MesPyBTM (351 mg, 0.581 mmol, 39%, mp 192–195 °C) and αH-Mes$_2$PyBTM (252 mg, 0.367 mmol, 24%, mp 122–124 °C).

αH-MesPyBTM (1 : 1 mixture of two conformers). ^{1}H NMR (400 MHz, CDCl$_3$, ppm): δ 8.50 (s, 0.5H), 8.49 (s, 0.5H), 8.38 (s, 0.5H), 8.37 (s, 0.5H), 7.41 (d, J = 2.2 Hz, 0.5H), 7.39 (d, J = 2.2 Hz, 0.5H), 7.29 (d, J = 2.2 Hz, 0.5H), 7.25 (d, 0.5H), 7.16 (d, J = 1.7 Hz, 0.5H), 7.15 (d, J = 1.7 Hz, 0.5H), 7.04 (d, J = 1.7 Hz, 0.5H), 7.01 (d, J = 1.7 Hz, 0.5H), 6.93 (s, 2H), 6.80 (s, 1H), 2.32 (s, 3H), 2.02–2.00 (m, 6H).

^{13}C NMR (100 MHz, CDCl$_3$, ppm): δ 149.7, 149.5, 147.9, 147.8, 144.2, 144.2, 143.1, 143.1, 138.1, 138.0, 137.8, 137.5, 137.4, 137.4, 137.4, 136.8, 135.8, 135.7, 135.6, 134.6, 134.6, 134.2, 134.2, 133.7, 133.6, 133.3, 132.2, 132.0, 131.4, 131.1, 130.5, 130.0, 129.7, 129.5, 128.8, 128.5, 128.4, 50.0, 21.2, 20.7.

Elemental analysis calcd for C$_{27}$H$_{18}$Cl$_7$N: C 53.64, H 3.00, N 2.32; found: C 53.92, H 3.04, N 2.25.

HRMS (MALDI-TOF MS positive mode) m/z: [MH]$^+$ calcd for C$_{27}$H$_{19}$Cl$_7$N$^+$ 601.93317; found 601.93316.

αH-Mes$_2$PyBTM. ^{1}H NMR (400 MHz, CDCl$_3$, ppm): δ 8.51 (s, 1H), 8.38 (s, 1H), 7.19 (d, J = 1.7 Hz, 1H), 7.16 (d, J = 1.7 Hz, 1H), 7.06 (d, J = 1.7 Hz, 1H), 7.02 (d, J = 1.7 Hz, 1H), 6.94 (s, 4H), 6.91 (s, 1H), 2.32 (s, 6H), 2.07–2.02 (m, 12H)

^{13}C NMR (100 MHz, CDCl$_3$, ppm): δ 149.6, 147.8, 144.8, 142.9, 142.8, 137.7, 137.7, 137.6, 137.4, 137.0, 136.9, 135.9, 135.7, 134.7, 133.8, 132.9, 132.5, 131.5, 131.0, 129.6, 129.5, 128.4, 50.3, 21.2, 20.7.

Elemental analysis calcd for C$_{36}$H$_{29}$Cl$_6$N: C 62.82, H 4.25, N 2.03; found: C 63.06, H 4.32, N 1.98.

HRMS (MALDI-TOF MS positive mode) m/z: [MH]$^+$ calcd for C$_{36}$H$_{30}$Cl$_6$N$^+$ 686.05039; found 686.05075.

Synthesis of MesPyBTM

Under an argon atmosphere, αH-MesPyBTM (76.2 mg, 0.126 mmol) was dissolved in dry THF (~4 mL), and tBuOK in THF (1M solution, 0.2 mL, 1.6 eq.) was added. The reaction mixture was stirred overnight in the dark. Silver nitrate (61.3 mg, 0.361 mmol) in acetonitrile (1.5 mL) was added and stirred for 2.5 h. The reaction mixture was filtered, evaporated, and purified by flash chromatography on silica gel (CHCl$_3$: hexane = 1 : 1) and

dried *in vacuo* to afford MesPyBTM (74.1 mg, 0.123 mmol, 97%) as a red solid (mp 99–100 °C).

HRMS (MALDI-TOF MS negative mode) m/z: [M]$^-$ calcd for C$_{27}$H$_{17}$Cl$_7$N$^-$ 599.91862; found 599.91850.

Synthesis of Mes$_2$PyBTM

Under an argon atmosphere, αH-Mes$_2$PyBTM (60.7 mg, 0.0882 mmol) was dissolved in dry THF (~3 mL), and tBuOK in THF (1M solution, 0.15 mL, 1.7 eq.) was added. The reaction mixture was stirred overnight in the dark. Silver nitrate (59.6 mg, 0.351 mmol) in acetonitrile (1.5 mL) was added and stirred for 2 h. Chloroform was added to the mixture and filtered on a celite pad. The solvent was evaporated and the reaction mixture was purified by silica gel column chromatography (CHCl$_3$: hexane = 2 : 1) and dried *in vacuo* to afford Mes$_2$PyBTM (52.4 mg, 0.0762 mmol, 86%) as a red solid (mp 122–125 °C).

HRMS (MALDI-TOF MS negative mode) m/z: [M]$^-$ calcd for C$_{36}$H$_{28}$Cl$_6$N$^-$ 684.03584; found 684.03660.

Synthesis of αH-Mes$_2$F$_2$PyBTM

In a Schlenk tube, αH-F$_2$PyBTM (488 mg, 1.00 mmol), 2,4,6-trimethylphenylboronic acid (494 mg, 3.01 mmol), and Pd(dtbpf)Cl$_2$ (53.1 mg, 0.0815 mmol), were put under an argon atmosphere. The degassed K-EL 2 wt% : toluene (9 : 1 v/v) emulsion (3.6 mL) was added, and the mixture was heated at 70 °C. Degassed triethylamine (0.85 mL, 6.1 mmol) was finally added, and the reaction mixture was stirred at 70 °C overnight. The reaction mixture was cooled down to room temperature, dichloromethane was added, and filtered on a celite pad. The solvent was evaporated and purified by silica gel column chromatography (CHCl$_3$: hexane = 1 : 1). The mixture (402 mg) was separated by GPC (CHCl$_3$), and recrystallization from dichloromethane–methanol gave pure αH-Mes$_2$F$_2$PyBTM (114 mg, 0.174 mmol, 17%, mp 219–221 °C).

^{1}H NMR (400 MHz, CDCl$_3$, ppm): δ 8.36 (s, 1H), 8.24 (s, 1H), 7.12 (s, 4H), 6.93 (s, 4H), 6.85 (s, 1H), 2.32 (s, 6H), 2.04 (s, 12H).

^{13}C NMR (100 MHz, CDCl$_3$, ppm): δ 142.8, 137.7, 136.6, 135.9, 135.8, 135.4, 135.1, 133.7, 133.5, 132.2, 130.5, 128.4, 125.4, 125.3, 125.1, 42.3, 21.2, 20.7.

Elemental analysis calcd for C$_{36}$H$_{29}$Cl$_4$F$_2$N: C 65.97, H 4.46, N 2.14; found: C 66.00, H 4.44, N 2.10.

HRMS (MALDI-TOF MS positive mode) m/z: [MH]$^+$ calcd for C$_{36}$H$_{30}$Cl$_4$F$_2$N$^+$ 654.10949; found 654.10945.

Synthesis of Mes$_2$F$_2$PyBTM

Under an argon atmosphere, αH-Mes$_2$F$_2$PyBTM (28 mg, 0.043 mmol) was dissolved in dry THF (3 mL), and tBuOK in THF (1M solution, 0.1 mL, 2.3 eq.) was added. The reaction mixture was stirred overnight in the dark. Silver nitrate (35.5 mg, 0.209 mmol) in acetonitrile (0.7 mL) was added and stirred for 3 h. Chloroform was added to the mixture and filtered on a celite pad. The solvent was evaporated and the reaction mixture was purified by silica gel column chromatography (CHCl$_3$: hexane = 1 : 1) and dried *in vacuo* to afford Mes$_2$F$_2$PyBTM (25.6 mg, 0.0391 mmol, 90%) as a red solid (mp 107–109 °C).

HRMS (MALDI-TOF MS positive mode) m/z: $[M]^+$ calcd for $C_{36}H_{28}Cl_6NF_2^+$ 652.09384; found 652.09347.

Data availability

The datasets supporting this article have been uploaded as part of the ESI.†

Author contributions

Y. H. conceived the project. Y. H. and R. K. prepared the compounds. W. O. and Y. H. conducted the DFT calculations. Y. H., R. M. and R. K. carried out the photophysical measurements. T. S. and W. O. contributed to the theoretical interpretation. Y. H. and W. O. wrote the original draft, and R. M., T. K., T. S. and K. U. reviewed and edited.

Conflicts of interest

There are no conflicts to declare.

Acknowledgements

Notes and references

1 P. Murto and H. Bronstein, *J. Mater. Chem. C*, 2022, **10**, 7368–7403.

2 R. Matsuoka, A. Mizuno, T. Mibu and T. Kusamoto, *Coord. Chem. Rev.*, 2022, **467**, 214646.

3 Q. Peng, A. Obolda, M. Zhang and F. Li, *Angew. Chem., Int. Ed.*, 2015, **54**, 7091–7095.

4 X. Ai, E. W. Evans, S. Dong, A. J. Gillett, H. Guo, Y. Chen, T. J. H. Hele, R. H. Friend and F. Li, *Nature*, 2018, **563**, 536–540.

5 Y. Hattori, S. Kimura, T. Kusamoto, H. Maeda and H. Nishihara, *Chem. Commun.*, 2018, **54**, 615–618.

6 C.-H. Liu, E. Hamzehpoor, Y. Sakai-Otsuka, T. Jadhav and D. F. Perepichka, *Angew. Chem., Int. Ed.*, 2020, **59**, 23030–23034.

7 M. Ballester and G. de la Fuente, *Tetrahedron Lett.*, 1970, **11**, 4509–4510.

8 O. Armet, J. Veciana, C. Rovira, J. Riera, J. Casteñer, E. Molins, J. Rius, C. Miravitlles, S. Olivella and J. Brichfeus, *J. Phys. Chem.*, 1987, **91**, 5608–5616.

9 M. A. Fox, E. Gaillard and C.-C. Chen, *J. Am. Chem. Soc.*, 1987, **109**, 7088–7094.

10 S. R. Ruberu and M. A. Fox, *J. Phys. Chem.*, 1993, **97**, 143–149.

11 Y. Hattori, T. Kusamoto and H. Nishihara, *Angew. Chem., Int. Ed.*, 2014, **53**, 11845–11848.

12 S. Kimura, T. Kusamoto, S. Kimura, K. Kato, Y. Teki and H. Nishihara, *Angew. Chem., Int. Ed.*, 2018, **57**, 12711–12715.

13 S. Kumar, Y. Kumar, S. K. Keshri and P. Mukhopadhyay, *Magnetochemistry*, 2016, **2**, 42.

14 A. Ghirri, C. Bonizzoni, F. Troiani, N. Buccheri, L. Beverina, A. Cassinese and M. Affronte, *Phys. Rev. A*, 2016, **93**, 063855.

15 K. Kato, S. Kimura, T. Kusamoto, H. Nishihara and Y. Teki, *Angew. Chem., Int. Ed.*, 2019, **58**, 2606–2611.

16 S. Kimura, S. Kimura, K. Kato, Y. Teki, H. Nishihara and T. Kusamoto, *Chem. Sci.*, 2021, **12**, 2025–2029.

17 Z. Zhou, C. Qiao, J. Yao, Y. Yan and Y. S. Zhao, *J. Mater. Chem. C*, 2022, **10**, 2551–2555.

18 Y. Hattori, T. Kusamoto and H. Nishihara, *RSC Adv.*, 2015, **5**, 64802–64805.

19 Y. Hattori, T. Kusamoto and H. Nishihara, *Angew. Chem., Int. Ed.*, 2015, **54**, 3731–3734.

20 Y. Hattori, T. Kusamoto, T. Sato and H. Nishihara, *Chem. Commun.*, 2016, **52**, 13393–13396.

21 Y. Hattori, R. Kitajima, R. Matsuoka, T. Kusamoto, H. Nishihara and K. Uchida, *Chem. Commun.*, 2022, **58**, 2560–2563.

22 V. Gamero, D. Velasco, S. Latorre, F. López-Calahorra, E. Brillas and L. Juliá, *Tetrahedron Lett.*, 2006, **47**, 2305–2309.

23 D. Velasco, S. Castellanos, M. López, F. López-Calahorra, E. Brillas and L. Juliá, *J. Org. Chem.*, 2007, **72**, 7523–7532.

24 S. Castellanos, D. Velasco, F. López-Calahorra, E. Brillas and L. Juliá, *J. Org. Chem.*, 2008, **73**, 3759–3767.

25 S. Dong, W. Xu, H. Guo, W. Yan, M. Zhang and F. Li, *Phys. Chem. Chem. Phys.*, 2018, **20**, 18657–18662.

26 H. Guo, Q. Peng, X.-K. Chen, Q. Gu, S. Dong, E. W. Evans, A. J. Gillett, X. Ai, M. Zhang, D. Credgington, V. Coropceanu, R. H. Friend, J.-L. Brédas and F. Li, *Nat. Mater.*, 2019, **18**, 977–984.

27 A. Heckmann, S. Dümmler, J. Pauli, M. Margraf, J. Köhler, D. Stich, C. Lambert, I. Fischer and U. Resch-Genger, *J. Phys. Chem. C*, 2009, **113**, 20958–20966.

28 Y. Beldjoudi, M. A. Nascimento, Y. J. Cho, H. Yu, H. Aziz, D. Tonouchi, K. Eguchi, M. M. Matsushita, K. Awaga, I. Osorio-Roman, C. P. Constantinides and J. M. Rawson, *J. Am. Chem. Soc.*, 2018, **140**, 6260–6270.

29 M. Ito, S. Shirai, Y. Xie, T. Kushida, N. Ando, H. Soutome, K. J. Fujimoto, T. Yanai, K. Tabata, Y. Miyata, H. Kita and S. Yamaguchi, *Angew. Chem., Int. Ed.*, 2022, e202201965.

30 S. Mattiello, F. Corsini, S. Mecca, M. Sassi, R. Ruffo, G. Mattioli, Y. Hattori, T. Kusamoto, G. Griffini and L. Beverina, *Mater. Adv.*, 2021, **2**, 7369–7378.

31 S. Kimura, M. Uejima, W. Ota, T. Sato, S. Kusaka, R. Matsuda, H. Nishihara and T. Kusamoto, *J. Am. Chem. Soc.*, 2021, **143**, 4329–4348.

32 G. Scalmani and M. J. Frisch, *J. Chem. Phys.*, 2010, **132**, 114110.

33 R. Improta, V. Barone, G. Scalmani and M. J. Frisch, *J. Chem. Phys.*, 2006, **125**, 054103.

34 A. Abdurahman, T. J. H. Hele, Q. Gu, J. Zhang, Q. Peng, M. Zhang, R. H. Friend, F. Li and E. W. Evans, *Nat. Mater.*, 2020, **19**, 1224–1229.

35 Y. Zhao, A. Abdurahman, Y. Zhang, P. Zhang, M. Zhang and F. Li, *CCS Chem*, 2022, **4**, 722–731.

36 S. Kimura, A. Tanushi, T. Kusamoto, S. Kochi, T. Sato and H. Nishihara, *Chem. Sci.*, 2018, **9**, 1996–2007.

37 T. L. Chu and S. I. Weissman, *J. Chem. Phys.*, 1954, **22**, 21–25.

38 E. Cho, V. Coropceanu and J.-L. Brédas, *J. Am. Chem. Soc.*, 2020, **142**, 17782–17786.

39 G. Fisher, *Vibronic Coupling: The Interaction between the Electronic and Nuclear Motions*, Academic Press, London, 1984.

40 T. Azumi and K. Matsuzaki, *Photochem. Photobiol.*, 1977, **25**, 315–326.

41 M. Uejima, T. Sato, D. Yokoyama, K. Tanaka and J.-W. Park, *Phys. Chem. Chem. Phys.*, 2014, **16**, 14244–14256.

42 T. Kato, N. Haruta and T. Sato, *Vibronic coupling density: Understanding molecular deformation*, Springer, Singapore, 2014.

43 R. Englman and J. Jortner, *Molecular. Phys.*, 1970, **18**, 145–164.

44 R. A. Velapoldi and H. H. Tønnesen, *J. Fluoresc.*, 2014, **14**, 465–472.